UNIVERSITI PUTRA MALAYSIA

PHASE FORMATION, CRYSTAL STRUCTURE AND MICROSTRUCTURE OF MgB2 WITH ADDITION OF S

NURUL ATIKA FARIHAH BINTI MOHD SHAFIE

PHASE FORMATION, CRYSTAL STRUCTURE AND MICROSTRUCTURE OF MgB_2 WITH ADDITION OF S

NURUL ATIKA FARIHAH BINTI MOHD SHAFIE

BACHELOR OF SCIENCE IN PHYSICS WITH HONORS

UNIVERSITI PUTRA MALAYSIA

2022

PHASE FORMATION, CRYSTAL STRUCTURE AND MICROSTRUCTURE OF MgB_2 WITH ADDITION OF S

By

NURUL ATIKA FARIHAH BINTI MOHD SHAFIE

198234

Thesis Submitted to the Department of Physics, Universiti Putra Malaysia, in partial Fulfilment of the Requirements for the Degree of Bachelor of Science in Physics (Honors)

January 2022

ABSTRACT

PHASE FORMATION, CRYSTAL STRUCTURE AND MICROSTRUCTURE OF MgB_2 WITH ADDITION OF S

By

NURUL ATIKA FARIHAH BINTI MOHD SHAFIE

2021

Supervisor : Chen Soo Kien (Assoc. Prof. Dr.)

Department : Physics, Faculty of Science

The phase formation, crystal structure and microstructure of MgB_2 with the addition of S was determined in this study. All the samples were sintered in 800°C. X-ray diffraction (XRD) data indicates that MgO was the main phase and unfortunately MgB_2 acted as secondary phase in all samples. The weight fraction of MgB_2 was found to decrease as the number of mole of S added increase. The higher the number of mol S added, the average grains size decreased. However, sample with addition S 0.02mol indicating the smallest grain growth which is 0.438μm. The density value increased and reach the optimum value when added with 0.02mol S. However, the density of the sample decreases as number of S added increased.

ABSTRAK

PEMBENTUKAN FASA, STRUKTUR KRISTAL DAN STRUKTUR MIKRO MgB_2 DENGAN TAMBAHAN S

Oleh

NURUL ATIKA FARIHAH BINTI MOHD SHAFIE

2022

Penyelia : Chen Soo Kien (Prof. Madya. Dr.)

Jabatan : Fizik, Fakulti Sains

Dalam kajian ini, pembentukan fasa, struktur hablur dan mikrostruktur MgB_2 dengan penambahan S telah ditentukan. Semua sampel telah melalui proses persinteran dengan suhu 800°C. Melalui pembelauan sinar (XRD), data yang diperoleh menunjukkan bahawa MgO adalah fasa utama dan malangnya MgB_2 bertindak sebagai fasa sekunder dalam semua sampel. Pecahan berat MgB_2 didapati berkurangan apabila bilangan mol S ditambah bertambah. Semakin tinggi jumlah mol S ditambah ke dalam sampel, saiz purata butiran berkurang. Walau bagaimanapun, sampel dengan penambahan S 0.02mol menunjukkan pertumbuhan bijian terkecil iaitu 0.438µm. nilai ketumpatan meningkat dan mencapai nilai optimum apabila ditambah dengan 0.02mol S. Ketumpatan sampel berkurangan apabila jumlah berat S ditambah bertambah.

ACKNOWLEDGEMENTS

In the name of Allah, the Most Gracious and the Most Merciful.

First and foremost, I would like to express my deepest gratitude and appreciation to my project supervisor, Assoc. Prof. Dr Chen Soo Kien who made this work possible. His guidance and advice motivated me to going through all the stages of writing my project.

Furthermore, I would like to express my appreciation to the postgraduate student in the superconductor lab, Miss Nur Hidayah Binti Mohd Hapipi for her guidance from the first day entering the lab until the end of this project's journey. I would also to thank my lab partner, Nur Zahidah Binti Abdul Rahman for letting this journey an enjoyable moment and for your comments and suggestions, thank to you. I would also to thank to all my close friend that always be my backbone to finish this study.

Finally, I would like to thank my family members for all the moral support and unstoppable Du'a for me to finish this study successfully, thanks to all of you.

TABLE OF CONTENT

LIST OF FIGURES

LIST OF TABLES

Table **page**

CHAPTER 1

INTRODUCTION

1.1 BACKGROUND AND HISTORY

A superconductor is the material that conducts electricity with no resistance. During the process, there was no energy released when it reached their critical temperature. Superconductivity was first discovered by Dutch physicist Heike Kamerlingh Onnes of Leiden University in 1911 when he cooled the mercury to the temperature of liquid helium, 4.2-degree Kelvin (4.2 K) its resistance vanished.(Van Delft & Kes, 2011).

In 1933, Walter Meissner and Robert Ochsenfeld discovered Meissner effect (Weh, n.d.). The Meissner effect is another name of diamagnetism, a magnetic link to superconductivity. When a material switches from normal to superconducting, magnetic fields are actively excluded from its interior. When a weak external magnetic field is supplied to a superconductor, it expels the applied magnetic field, leaving no magnetic flux throughout its body.

In 1935, brothers Fritz and Heinz London has proposed London theory. This theory describes how a magnetic field must be shaped in order to meet the Meissner effect's essential conditions: no magnetic field within the conductor, and electric currents may only flow from the conductor surface to a depth of a certain distance. London model shows that when a magnetic field is applied to a sample and the applied flux is excluded throughout its interior, the static flux survives inside a sheath of depth at the sample's surface; its magnitude diminishes exponentially towards the superconductor's core (Michael & Davor, 1992). In 1950, Vitaly Ginzburg and Lev Landau introduced Ginzburg-Landau theory, which studies the physical properties of superconductor (Baturina & Vinokur, 2014). This theory combines Landau's theory of second-order phase transitions with a Schrödinger-like wave equation to describe the macroscopic features of superconductors with tremendous success.

Discovery of high T_c superconductor brought a revolution in the field of science and technology. In 1957, Alexi Abrikosov discovered that superconductor can be grouped as type-I and Type-II. In the same year, John Barden, Leon Cooper and John Schrieffer discovered a microscopy theory of superconductivity called BCS theory (Rodriguez, 2017). BCS theory

claims that at low temperatures, electrons flow through superconductors in pairs, avoiding most of the heat-generating collisions in the conductors. MgB_2, was discovered to be superconducting at a surprisingly high temperature, 39K by Akimitsu in 2011 (Tomsic et al., 2007).

When a material changes from a conductor to a superconductor, the material is in a superconducting state. When the temperature of the material drops below the critical temperature, the resistance of the material drops sharply to zero. This means that the material is superconducting and has no resistance. When the applied magnetic field H exceeds the critical magnetic field Hc, the superconductor turns into a normal conductor. Even in the superconducting state, the material experienced a critical magnetic field. The critical magnetic field is inversely proportional to temperature. As the temperature rises, the value of the critical magnetic field decreases.

1.2 TYPE-I AND TYPE-II SUPERCONDUCTOR

Type-I superconductors are also referred to as soft superconductors because they easily lose their superconducting state when subjected to a low-intensity magnetic field. As a result, the transition of type-I superconductors from normal to superconducting state occurs instantaneously and the technical applications for type-I superconductors are limited. Except for niobium, vanadium, and technetium, all pure element superconductors are classified as type-I. Besides, type-I superconductors have low critical temperature and low critical magnetic field. Type-I superconductors obeyed the Meissner effect perfectly; the magnetic field cannot infiltrate in it. When the applied field strength exceeds a critical value, superconductivity is abruptly destroyed through a first order phase transition.

Type-II superconductors are also referred to as hard superconductors because the superconducting state is not easily lost due to an external magnetic field. In general, the external magnetic field causes a gradual but not abrupt transition from a superconducting to a normal state. Type-II superconductors begin to lose their superconductivity at lower critical magnetic fields and completely lose their superconductivity at upper critical magnetic fields. Type-II

superconductors are typically ceramic alloys and complex oxides. Type-II superconductors have high critical temperature and high critical magnetic field. Type-II superconductors obeyed the Meissner effect partly; the magnetic field can infiltrate in it. Magnesium diboride (MgB2) is a type-II superconductor. Figure 1.1 shows the magnetisation of type-I and type-II superconductor.

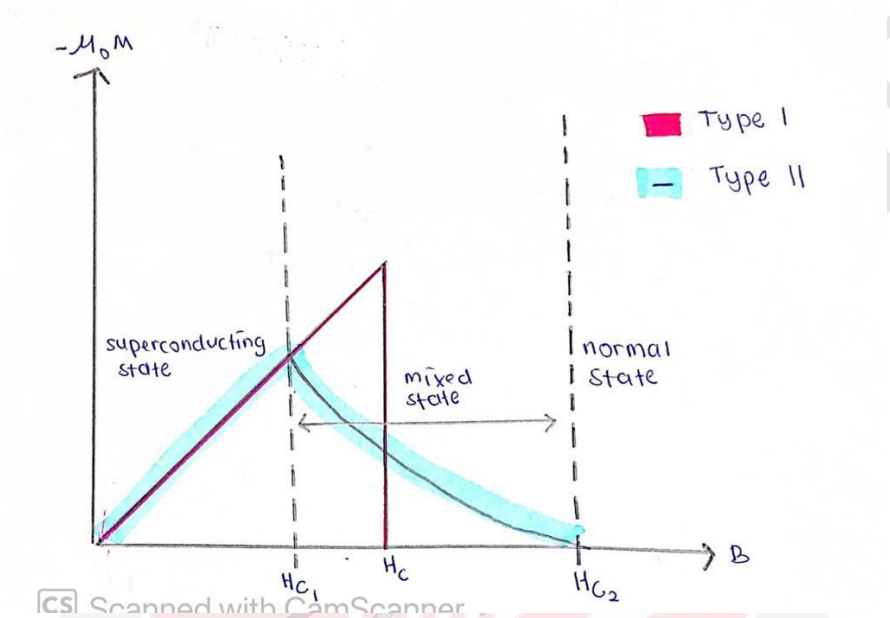

Figure 1.1: magnetisation of type-I and type-II superconductor as a function of magnetic field.

1.3 APPLICATIONS OF SUPERCONDUCTOR

The development of superconductors has been a great benefit to humankinds. It has a wide range of applications in numerous disciplines of science and technology due to its unique zero resistivity feature. Nowadays, superconductors have been used in telecommunication, medical, transportation, space and power transmission. Firstly, the Meissner effect was applied to magnetic levitation device (MAGLEV). Superconductors produce a magnetic field that repels magnets and the repulsion can be more powerful than gravity, resulting in levitation. Superconductor also used for medical purpose such as magnetic resonance image (MRI). Traditional MRI relies on the notion that protons have spin and consequently a magnetic moment and that a radio frequency pulse of magnetic field causes protons in the patient to process in the direction of the static magnetic field produced by the MRI machine's super

conductive magnet. Superconductivity also beneficial for motors and generators. MgB_2 provides the possibility for better power densities, larger temperature margins, and smaller weight coils for the superconducting homopolar motor. In power transmission, due to the zero-resistance property of the super conducting wires, all the electric motors could be improved in proficiency. Lastly, defence application. Initiative for a strategic defence, instead of anticipated nuclear detonations, laser technology might derive its megawatt energy bursts from super conduction storage units (Tomsic et al., 2007).

1.4 PROBLEM STATEMENT

Considering non-oxide-based superconductors, MgB_2 is one of those with a high critical temperature at 39 K. Various types of chemical doping of magnesium diboride (MgB_2) have been researched and published in the recent years. In order to enhance the critical current characteristics of MgB_2, numerous elements and compounds have been doped. Carbon is the most effective dopant for MgB_2 because it enhances the rate of impurity scattering, boosts the higher critical field and has high-field critical current. However, based on my observation, there are only a few researches on MgB2 with sulphur (S) addition. At high pressures (more than 100 GPa), elemental sulphur exhibits a superconducting phase with critical temperatures of up to 20 K (M. Monni et all., 2017). This shows that S has lower critical temperature than MgB_2 Additionally, S is a nonmagnetic element with a relatively low melting point (~ 112 °C). Addition of S to MgB_2 compound is expected to enhance the critical current density and reduce the impurities of MgO. Hence, investigation of S doping on phase formation and crystal structure of MgB_2 is crucial to ascertain the influence of S on the superconducting properties of MgB_2. There are two routes for synthesizing MgB_2 namely the in-situ and ex-situ reaction method. So far, most of doped MgB_2 samples were synthesized by using in-situ method since it is more effective than the ex-situ method for sintering process and doping. The samples obtained from the in-situ reaction method have better grain connectivity and thus high critical current density. In this research, the samples were prepared by using in-situ reaction method and effect of S addition on phase formation, crystal structure and microstructure evolution of MgB_2 are studied.

1.5 OBJECTIVES

I. To study the effect of addition of S on phase formation of MgB_2.

II. To investigate crystal structure properties in S added MgB_2.

III. To analysis microstructure evolution of MgB_2 as a result of S addition.

1.6 THESIS ORGANIZATION

This research carried out to study the phase formation, crystal structure and microstructure of MgB2 with addition of S. chapter 1 illustrates the background and history of superconductor MgB2, properties of superconductor and types of superconductors. It is followed by problem statement and objectives of this project. Chapter 2 outlines the literature review of previous studies on effect of addition S on phase formation, crystal structure properties and microstructure evolution of MgB2. Chapter 3 explains the methodology of this project. It consists material and apparatus use, raw material calculations, procedures and the characterisation that used for this project. Chapter 4 discuss the obtained results. Lastly, chapter 5 concludes the research.

CHAPTER 2

LITERATURE REVIEW

2.1 BASIC PROPERTIES AND STRUCTURE OF MgB_2

Low temperature superconductors like NbTi and Nb_3Sn are widely used nowadays. After the discovery of MgB_2, which has a relatively high critical temperature (T_c), there has been increased interest in using MgB_2 in industrial applications. Akimitsu and his group had found the superconductivity in magnesium diboride in 2001 (Van Delft & Kes, 2011). MgB_2 is superconducting below 39 K. It is a common binary boride that crystallises in the AlB_2 structure. With the appearance of dark grey, MgB_2 is an inorganic compound that is not soluble in water. The high T_c of MgB_2 is nearly to the theoretical value predicted by BCS theory and can be considered as a non-conventional superconductor. Table 2.1 shows T_c values of some metal borides by Bor et al. (2017).

.

Chemical Composition	Critical Temperature (T_c)
MgB_2	**39**
TaB_2	9.5
$Nb_{0.76}B_2$	9.2
$MoB_{2.5}$	8.1
$NbB_{2.5}$	6.4
ZrB2	5.5
BeB_2	0.79
NbB_2	0.62
Nb_3Ge	**23.2**

Table 2.1: T_c values of some metal borides (Bor et al., 2017).

MgB_2 possesses exceptional thermodynamic and transport characteristics, as well as the isotope effect, band structures, promising critical current density, doping ability, and pressure

effect. MgB_2 is a medium-temperature superconductor (MTS) with great potential because of its unique properties, including a simple crystal structure, low material cost and lower anisotropy. Furthermore, MgB_2 is a basic metallic combination made up of two light elements, Mg and B, making it a promising option for next-generation superconducting materials that can function at a temperature of 15-20 K without relying on liquid helium.

MgB_2 crystallises hexagonally in an AlB_2 type of structure, according to structural refinement determined from single-crystal X-ray diffraction investigation, with a = 3.0849 Å and c = 3.5187 Å (Bor et al., 2017). The magnesium atoms are centred above and below the hexagonal graphite-type boron layers in MgB_2, which are separated by hexagonal close-packed layers of magnesium. In order to forming an ionic bond, magnesium atoms donate their valence electrons to the boron planes. Boron atom indicates a strong anisotropy in the B-B length (Bor et al., 2017). Three sigma bonds and two pi bonds form the band structure of MgB_2. Strong two-dimensional (2D) covalent bonds and three-dimensional (3D) metallic bonding occur between the layers, holding the in-plane boron atoms together. Both the covalent (2D) sigma band and the metallic (3D) pi band contribute to the electronic density of state at the Fermi level, as well as the normal state conductivity (Ravindran et al.,2001). The electrical structure at the fermi level is governed by the hexagonal network of the two-dimensional boron sheet, and the boron layer is thought to be responsible for superconductivity (Choi et al., 2002). Figure 2.1 illustrates the crystal structure of MgB_2.

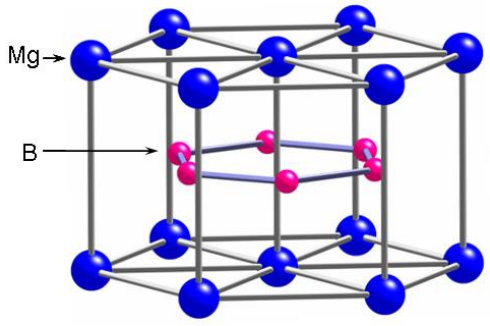

Figure 2.1: Crystal structure of MgB_2, a=3.086 Å and c=3.524 Å **(**Xu et al., 2011) .

2.2 SYNTHESIS OF MGB_2 USING IN-SITU REACTION METHOD

The in-situ method employs lower heat treatment temperatures, allowing for a wider range of metallic sheaths and hence more material adaptability. However, because the initial Mg+2B mixture have a lower density than the MgB_2 phase, this process has the intrinsic issue of having a low final density. In the in-situ reaction process, the Mg particles melt and disperse into the B particles, turning the B particles into voids, resulting in lower bulk density and poor connectivity. Critical current density (J_c) of in-situ MgB_2 higher is higher than that of ex situ MgB_2 since the inter-grain coupling of in-situ MgB_2 is stronger as compared to the ex situ MgB_2. The low filling factor (about 65%) of Mg and B powders in in-situ manufactured MgB_2 wires has an impact on the porosity of the final MgB_2 compound (Shcherbakov, 2011). However, the packing factor of in-situ MgB_2 is lower than ex situ MgB_2 which affect the connectivity of grain coupling. Pan et al. (2003) studied that the grain size generated in in-situ MgB_2 superconductors is predicted to be two orders of magnitude bigger than that of ex situ particles. Furthermore, in-situ process uses unreacted MgB_2, thus, the ability for sintering is high and the make the doping process of impurities more effective compared with the ex situ MgB_2.

2.3 MICROSTRUCTURE OF MgB_2

Using the in-situ reaction technique for sample preparation, MgB_2 has a porous microstructure with huge spaces ranging in size from 10μm to 50μm. Before heat treatment, spaces filled with Mg particles become voids as a result of the interaction with B. Tanaka et al. (2012) state that the inter-grain coupling between MgB_2 grain of in-situ samples is high compared to ex situ samples where a strong linked network of MgB_2 is observed.

The electronic transport in superconductors is greatly influenced by grain boundaries in both the normal and superconducting states. High-angle grain boundaries, for example, operate as weak links in high-Tc cuprates, suppressing current-carrying capabilities even in smaller magnetic fields. The critical current (I_c) of a grain boundary has an unusual magnetic-field behaviour that is highly influenced by the curvature angle. I_c is relatively insensitive to an applied field in low-angle grain boundaries, which are limited by flux creep—these boundaries are linked strongly. The stronger connectivity of grain boundaries, the value of critical current density will increase. Insulating grain boundaries prevent supercurrent crossing them. Grain

boundaries operate as 'weak-links,' according to the Dimos data, which demonstrate that critical current density reduces with increasing misorientation angle in [001] tilt boundaries (Wang et al., 2017). A large number of grain boundaries guarantees that the sample contains the most pinning centres. The vortices start reorganising themselves as soon as the applied magnetic field starts breaking ‘weak connections' at the grain boundaries, resulting in a large Jc reduction.

The improved flux pinning and Jc are largely due to the decreased grain size and therefore higher density of grain boundary pinning centres of MgB_2 bulks synthesised at low temperature. It is known that the grain boundaries of superconducting MgB_2 form effective flux pinning sites. Fluxons travelling down grain boundary channels past fluxons kept motionless within the grains by high surface pinning can be the dissipation process in polycrystalline superconductors. A grain boundary in polycrystalline MgB_2 is the intersection of two grains, or crystallites. To have superconducting transport properties similar to those found in polycrystalline samples, bicrystal grain boundaries would need to include the complicated topology of polycrystalline grain boundaries as well as have surface pinning removed, which can be expected at the superconductor-air and superconductor-substrate interfaces in bicrystal systems. Tarasov et al. (2007) propose that the developing a MgB2 film over a bicrystalline magnesium oxide substrate orientated in the (111) plane (MgO (111)) to provide a stronger weak link.

2.4 ANISOTROPY

Anisotropy known as the property of a material to display variations in physical characteristics along distinct crystallographic axes. MgB_2 is suitable for applications due to its low anisotropy, long coherence length, and grain boundary transparency to current flowMgB_2 high anisotropic crystalline structure, which consists of triangular layers of magnesium atoms sandwiched between hexagonal layers of boron atoms, had been known for about 50 years before superconductivity was discovered in this binary compound (De Lima & Crdoso, 2003). Until the maximum pressure, MgB_2 remains completely hexagonal, with no signs of structural transition change. By using the two-gap Ginzburg-Landau theory, the upper critical field in MgB_2 was investigated. The upward temperature dependence of in-plane Hc_2 as well as the departure of its out-of-plane behaviour from the normal angular dependency may be attributed to the temperature change of the ratio of two gaps. With lowering temperature, Hc_2 's hexagonal in-plane modulations may change sign. Figure 2.2 shows upper critical field anisotropy. Figure 2.3 illustrate the pressure variation of the normalized hexagonal lattice constants a and c. the lattice parameter along c-axis drop quickly with pressure than along a-axis and demonstrate that the out-of-plane Mg-B bonds are much weaker than in-plane Mg-Mg bonds. The compressibility anisotropy reduces linearly with pressure shown in figure 2.4. Figure 2.5 shows that the dependency of Tc on the unit cell volume based on the critical temperature dependency on applied pressure, which was validated by compressibility data.

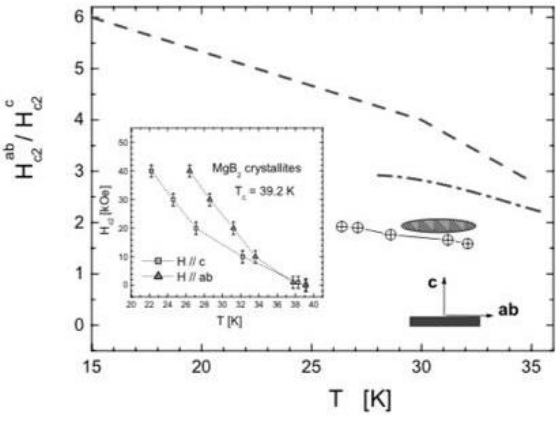

Figure 2.2: Anisotropy ratio of the upper critical field in MgB_2 **(**De Lima & Crdoso, 2003).

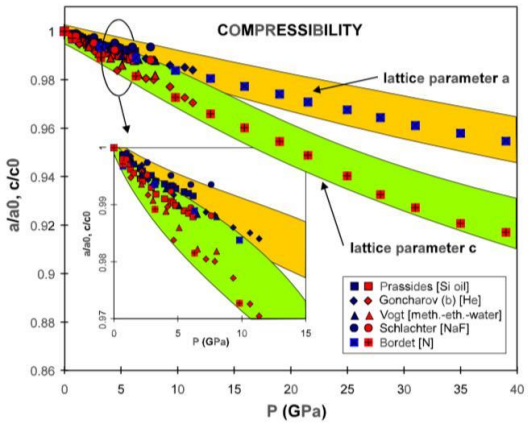

Figure 2.3: The normalized lattice parameters to the zero-pressure value versus applied pressure (*Buzea & Yamashita, 2001).*

2.5 PHASE FORMATION OF MgB_2

Figure 2.4 illustrates the The XRD pattern of pure MgB_2.

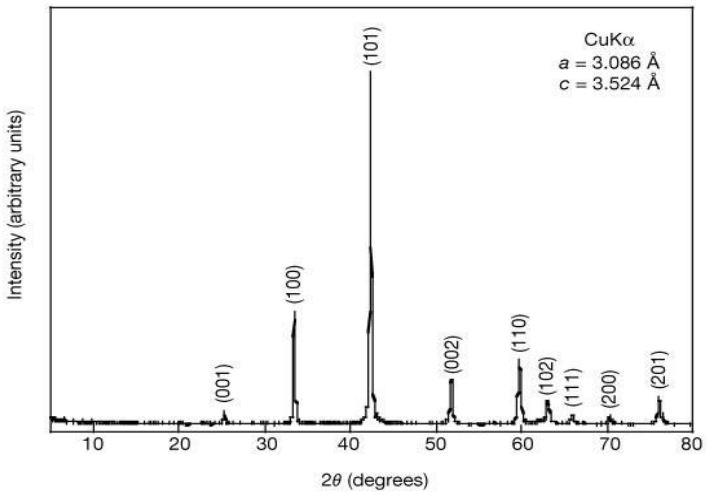

Figure 2.4: XRD pattern of pure MgB_2 (Nagamatsu et al., 2001).

The highest intensity peak of MgB_2 was recorded at $2\Theta = 42.6°$. The metallic Mg was represented as peak intensities at $2\Theta = 30°$ to 40°, which enhanced consistently as a function of the metallic Mg concentration. The sintering temperature was 1000°C, which is a very high temperature for the MgB_2 phase to develop. In in-situ reaction method, the pure Mg – B mixture, MgB_2 starts forming around 600°C. However, (Aksu, 2013) states that MgB_2 phase began to form at 530 °C and the amount of formed MgB_2 phase increased with the increase in the sintering temperatures up to 900 °C. The unreacted magnesium may reach temperatures around 648°C, and that the production of MgB_2 takes place only after the remaining Mg has melted. The amount of addition to the MgB_2 will affected the major phase of MgB_2 but does not affected the lattice parameter of MgB_2.

Sulphur (S) is a reactive compound that can react with hydrogen gas produce hydrogen sulphide. Hydrogen sulphide is an example of high temperature superconductor. Furthermore, various study shown that the sulphur-based material, which is sulphur trihydride (H_3S) in superconducting state with the highest transition temperature (203 K). The addition of S to the Mg and B powder combination have no influence on grain growth and does not impacts the MgB_2 lattice. However, the development of nanometre-sized secondary phase particles can be beneficial for flux pinning. The existence of an intermetallic compound (Mg_3Bi_2) characterises the Mg – Bi phase diagram, which forms eutectic systems with Mg and Bi at temperatures of 553°C and 260° respectively (Grivel et al., 2012). These characteristics make Bi, as well as Se, an ideal addition for lowering the MgB_2 formation temperature since it is more likely to induce Mg melting at lower temperatures than in the pure Mg-B system due to low solubility limit of Bi in Mg (maximum 1.12 at. % 553°C). based on data collected by Grivel et.al. for Bi phase formation, not all the Se react with Mg to form a substance before the eutectic temperature was reached. Based on the studies, the addition of S was predicted to the MgB_2 also lowered the MgB_2 formation temperature and reduce the impurities of MgO.

.

CHAPTER 3

METHODOLOGY

3.1 SAMPLE PREPARATION

In this work, in-situ solid state reaction was used for sample preparation. Five samples were prepared throughout this study. A total of 2g of high purity magnesium and boron was used for the first sample. For the second sample and onward, Sulphur powder was added according the mass calculated in the table below. Each element has different mass in each sample due to different number of mole of sulphur.

3.1.1 Apparatus

1. mortar & pestle
2. spatula
3. stainless steel tube
4. furnace
5. hydraulic press
6. electronic weigh balance
7. mould and die

Table 3.1 details for the raw chemical powder needed.

Raw chemical powder	Purity (%)	Manufacturer
Magnesium	99.7	Tangshan Wei Hao, China
Boron	95-97	Tangshan Wei Hao, China
sulphur	99.5	Alfa Aesar

3.2 Calculation of weight for each element with different x

Chemical equation of $MgB_2[S]_x$

Mg + 2B + xS $\longrightarrow$ $MgB_2[S]_x$

Atomic mass for (g/mol) for each element of different five samples:

Total molecular weight = 45.925 g/mol

Table 3.2.1: the calculation of weight for each element when x = 0.00 mol

Element	Formula weight (g/mol)	Mole	Molecular weight (g/mol)	Mass (1.6g)
Mg	24.305	1	24.305	0.8468
B	10.81	2	21.62	0.7532
S	32.06	0	0	0

Total molecular weight = 46.5662 g/mol

Table 3.2.2: the calculation of weight for each element when x = 0.02 mol

Element	Formula weight (g/mol)	Mole	Molecular weight (g/mol)	Mass (1.6g)
Mg	24.305	1	24.305	0.8351
B	10.81	2	21.62	0.7429
S	32.06	0.02	0.6412	0.022

Total molecular weight = 47.528 g/mol

Table 3.2.3: the calculation of weight for each element when x = 0.05 mol

Element	Formula weight (g/mol)	Mole	Molecular weight (g/mol)	Mass(1.6g)
Mg	24.305	1	24.305	0.8182
B	10.81	2	21.62	0.7278
S	32.06	0.05	1.603	0.0540

Total molecular weight = 48.1692 g/mol

Table 3.2.4: the calculation of weight for each element when x = 0.07 mol

Element	Formula weight (g/mol)	Mole	Molecular weight (g/mol)	Mass (1.6g)
Mg	24.305	1	24.305	0.8073
B	10.81	2	21.62	0.7181
S	32.06	0.07	2.2442	0.0745

Total molecular weight = 49.131 g/mol

Table 3.2.5: the calculation of weight for each element when x = 0.10 mol

Element	Formula weight (g/mol)	Mole	Molecular weight (g/mol)	Mass (1.6g)
Mg	24.305	1	24.305	0.7915
B	10.81	2	21.62	0.7041
S	32.06	0.1	3.206	0.1044

3.3 PROCEDURES

3.3.1 Grinding Process

According to the calculations at the tables above, the powder required for each sample was weighed using an electronic analytical weigh balance (Figure 3.1). Using a mortar and pestle, the powders of each sample were mixed and ground for at least 1 hour to ensure homogeneity (Figure 3.2).

Figure 3.1: electronic analytical weight balance

Figure 3.2: mortar and pestle

3.3.2 Palettization

In this process, ground powders were weighed and separated to 0.5g per portion. Acetone was used to clean the mould and die before using it. The powders were then loaded into a 13 mm diameter mould and pressed into a disc-shaped pellet using a hydraulic press system at 5 tons pressure for 5 minutes. The pellets as shown in Figure 3.3.

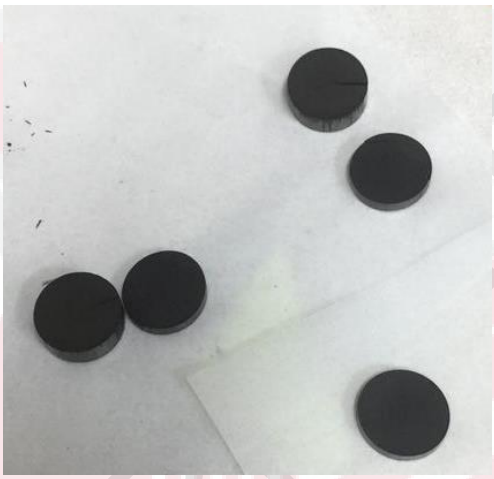

Figure 3.3: disc-shaped pellets

3.3.3 Sintering Process

After the pellets were prepared, they were ready for the sintering process. Five pellets of each sample were placed in a stainless-steel tube with one end sealed. The sample was put one by one to ensure there is no overlapping pellets inside the tube. The overlapping pellets may produce higher formation of impurities in the sample. The other end of the tube was sealed after the pellets were loaded inside. The stainless steel was then placed in an argon-gas-flowing furnace. To ensure a constant flow of argon gas through the furnace, one end of the furnace was connected to a water bath. The bubble that is released into the water bath at an approximate rate of one bubble per second. Each set of samples was sintered at 800°C for 1 hour at a rate of 5°C per minute of heating and cooling. Temperature control is important in the sintering

process because grain boundary diffusion and bulk diffusion are highly temperature dependent. Before undergo sintering process, the furnace was set and heated for 10 minutes to ensure that no oxygen left in the furnace. Temperature profile for the sample as shown in figure 3.4.

From 30-800°C,

(800 – 30)/5 = 154 min = 2.57 h

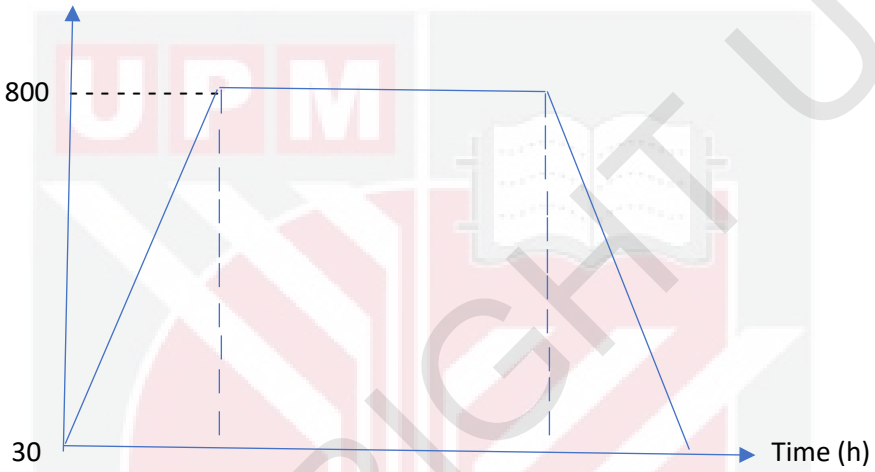

Figure 3.4: temperature versus time for sample sintered at 800°C

3.4 CHARACTERIZATION

3.4.1 X-Ray Diffraction

X-ray diffraction is a highly effective non-destructive method for characterising crystalline materials. XRD are used to describe structure, phase, preferred crystal orientation (texture), and other structural parameters such as average grain size, crystallinity, strain, and crystal defects. The constructive interference of monochromatic X-rays scattered at a particular angle from each set of lattice planes in the sample causes XRD peaks. The cathode ray tube produces these x-rays, which are then filtered to produce monochromatic radiation, collimated for

concentration, and directed to the sample. When the incident rays interact with the sample, they produce constructive interference (and diffracted rays) if the conditions meet Bragg's law. This law describes the relationship between the wavelength of electromagnetic radiation and the diffraction angle and lattice spacing in a crystalline sample.

$$n\lambda=2d \sin \theta \qquad \text{(eq. 3.1)}$$

where n is the integer, λ is the wavelength of the incident x-ray beam, d is the distance between atomic layers in a crystal and θ is the angle of the incidence. Figure 3.5 shows the bragg's law reflection by *Baskaran (2010).*

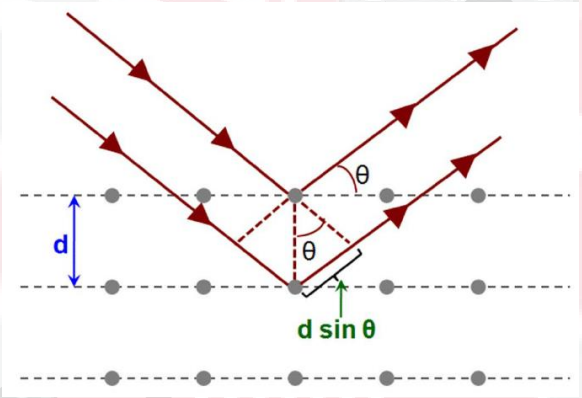

Figure 3.5: Bragg's law reflection (Baskaran, 2010).

Before the sample was sending to XRD analysis, the pelletized sample that had undergo sintering process then be grounded into powder. PW 3040/60 mpd x'pert pro panalytic Philips diffractometer with CuK_{α} radiation of wavelength, $\lambda=1.5406\dot{A}$ generated ate 40KV, 30mA was used. The sample were scanned through a range from $2\Theta=20°$ to $2\Theta=80°$ with 0.33 step size scanning. X'Pert Highscore Plus with the support of ICDD-PDF 2 database was used to analyse the XRD spectra.

3.4.2 Scanning Electron Microscopy (SEM)

The scanning electron microscopy (SEM) is a type of electron microscope that used to observe the surface microstructure of the sample. SEM creates a high-resolution and three-dimensional image by scanning a focussed electron beam over a surface. The electrons in the beam interact with the sample, generating a variety of signals that may be utilised to interpret surface topography and composition. High magnification image shows the grain size and shape with more details. In SEM, the components include electron sources, Column down which electrons travel with electromagnetic lenses, electron detector, sample chamber and the display to view the images. Figure 3.6 shows the schematic diagram of a SEM.

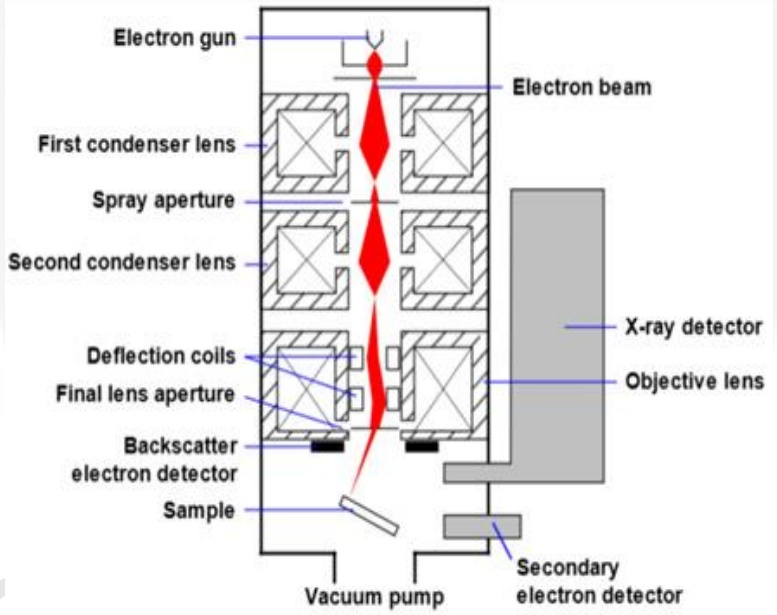

Figure 3.6: Schematic diagram of a Scanning Electron Microscope. (Microscope & Sem, n.d.)

Electrons are generated at the top of the column, propelled down the column, and passed through a series of lenses and apertures to produce a concentrated beam of electrons that strikes the sample's surface. Unless the microscope is built to function at low vacuums, the sample is put on a stage in the chamber region, and both the column and the chamber are evacuated by a combination of pumps. Scanning coils located above the objective lens regulate the location of the electron beam on the sample. These coils enable the beam to be scanned across the sample's surface. A variety of signals are created as a result of the electron-sample interaction. Detectors are then used to detect these signals. In this study, a scanning electron microscope (SEM-LEO

1455 VPSEM) equipped with energy dispersive X-ray spectrometer (EDX) was used. The samples were coated with a thin layer of gold before proceeding to microstructure observation to prohibit electrostatic charging. After that, the sample were put into the stage holder. The micrographs of the selected area were obtained from the EDX analysis. The measurement of grain size for each SEM image was calculated by using the image-J software.

3.4.3 Density Measurement

The density of each pellet can be calculated by dividing its mass by its volume. In this experiment, the solid densimeter was used to measure the density of the pellets. Before takes the reading, the tank of densimeter was filled with 1000ml distilled water. The pellet was put on the top of particle measuring assembly to measure the mass of the pallet on air. After that, the pellet was weighed on the floating body assembly to take the mass of the pellet in the water and its density. Figure below shown the solid densimeter that was used in the experiment.

Figure 3.7: solid densimeter

CHAPTER 4
RESULT AND DISCUSSION

4.1 XRD CHARACTERIZATION

The XRD pattern shown in Figure 4.1 illustrates the in-situ MgB2 reaction without addition and with 0.02mol. 0.05mol, 0.07mol and 0.1mol of S added that undergo sintering process at 800°C for one hour. All the samples were indexed to hexagonal unit cell and P6/mmm space group with a=b≠c with α=β=90° and γ=120° (ICSD file number: 98-010-6149). As shown in the figure, MgO was the major phase in all samples and MgB_2 as the secondary phase (ICSD: 98-004-7897). Based on the figure, sulphur added to the sample does not show any formation of phase probably due to its lower melting point of 112.8° that lead to it vaporized during sintering process at 800°C. However, The presence of higher fraction of MgO phase is due to the oxidation of metallic Mg (Science & Grivel, 2004). This fact is supported by Aksu (2013) that proposes the MgO phase formed due to the reaction of Mg with oxygen trapped in the aluminium container before undergo sintering process that yield MgO easily. Furthermore, The XRD analysis demonstrate that there was formation of MgB_4 (ICSD: 98-009-1660) in the sample of MgB_2 without addition. Savaskan et al. (2009) propose that the formation of MgB_4 was due to volatility of Mg that decomposed easily in high temperature. The presence of MgO and MgB_4 in the sample of MgB_2 without addition will decreases the value of critical current density (Matthews et al., 2020). However, MgB_4 phase does not formed in all samples with S addition.

Table 4.1 indicates the weight fraction of MgB_2, MgO and other impurities, which MgB_4 and B_2O that formed in every samples. Based on the table, as the number of mole S added increased, the formation of MgB_2 decreased except for the sample of MgB_2 with 0.05mol S added that showed highest formation of MgB_2 phase in this study but MgO still the major phase formed. The lower weight fraction of sample of MgB_2 without addition probably due to the decomposition of MgB_2 to MgB_4 phase (Savaskan et al., 2009). The result clearly showed that the addition of S increased the formation of MgO. However, a small amount of Boron Oxide (B_2O) was found in the sample of MgB_2 with addition 0.07mol of S (ICSD: 98-002-3491). Xu et al. (2008) proposed that the formation of B_2O was due to the oxidation of B powder in air. However, the presence of B_2O may decreases the formation of MgB_2 in the sample.

Table 4.2 indicate the lattice properties of in-situ reaction of MgB_2 without and with S addition respectively. The crystallite size and lattice strain of the samples were calculated using

Williamson-Hall plot method. In this method, five XRD peaks with the highest intensity of MgB_2 in each sample were chosen. The value of lattice strain can be obtained from the slope and the crystallite size from the intercept in a plot of the calculated FWHM, $\beta\cos\Theta$ against $4\sin\Theta$. As shown in the table, 0.02mol of S added does not influence the crystallite size and lattice strain value in the MgB_2 sample. The highest lattice strain and crystallite size was MgB_2 with 0.1mol of S addition whereas 0.11% and 96nm respectively. Furthermore, the results suggest that S added to the sample contributed to crystal growth. With the increased mol of addition S, the crystallite size and lattice strain also increase. The increases value of lattice strain probably due to higher lattice defect in the samples. Serquis et al. (2001) suggest that lattice defect such as vacancies, interstitials, substitutions, and stacking faults among grains boundary will lead to increase value of lattice strain.

The lattice parameters of the a-axis and c-axis for the sample MgB_2 without addition and with S addition were determined based on Rietveld method by using the X'pert Highscore Plus Software. The results were shown in table 4.2. Based on the table, lattice parameter along the a-axis ranging from 3.0810 Å to 3.0870 Å. However, the lattice parameter along the c-axis ranging from 3.5140 Å to 3.5280 Å. Interestingly, the a-lattice parameters were constant since the highest difference was 0.006 Å. Same goes with the c-lattice parameters, the highest difference was 0.014 Å. Since the difference was not very large, so the low doping achieved with this system was not expected to result in significant changes in the unit cell parameters. Lattice parameters along c-axis were higher than a-axis agreeing with Buzea & Yamashita (2001) that proposed this fact is because the out-of-plane Mg-B binding is much weaker than the in-plane Mg-Mg binding. The higher substitution of oxygen at the site could lead to higher values of c-axis (Tan et al., 2017).

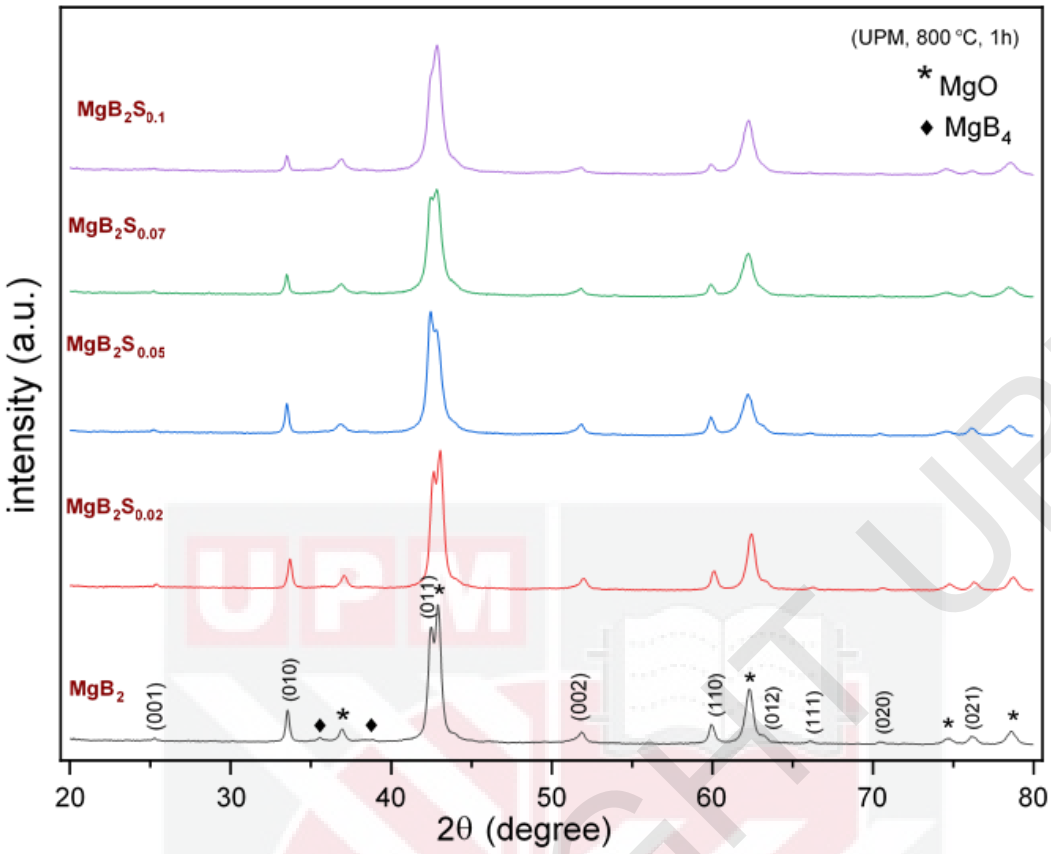

Figure 4.1: XRD pattern for each sample sintered at 800˚C

Table 4.1: Weight fraction of the phases formed in the samples.

Sample	weight fraction (%)			
	MgB_2	MgO	MgB_4	B_2O
MgB_2	46.72	52.04	1.24	0
$MgB_2S_{0.02}$	46.29	53.71	0	0
$MgB_2S_{0.05}$	47.30	52.70	0	0
$MgB_2S_{0.07}$	44.76	54.92	0	0.32
$MgB_2S_{0.1}$	37.75	62.25	0	0

Table 4.2: Crystallite size and lattice properties in five different samples.

Addition of S (mol)	Crystallite size (nm)	Lattice strain (%)	Lattice parameters (Å)	
			a=b	c
0.0	44	0.02	3.0860	3.5240
0.02	44	0.02	3.0810	3.5140
0.05	50	0.03	3.0870	3.5280
0.07	69	0.04	3.0870	3.5280
0.1	96	0.11	3.0850	3.5230

4.2 MICROSTRUCTURE

Figure 4.2 shows the SEM images of in-situ reaction MgB_2 without addition at magnification 7000x. Figure 4.2.2, figure 4.2.4, figure 4.2.6 and figure 4.2.8 illustrate the SEM images of in-situ MgB_2 with addition of sulphur for 0.02mol, 0.05mol, 0.07mol and 0.1mol, respectively. Aksu (2013) demonstrates that particles larger than 1 μm in size are Mg particles, and these particles are surrounded by particles smaller than 1 μm in size, which are attributed to amorphous particles. in the SEM images, MgB_4 grains, MgB_2 grains, pores and MgO impurities can be correlated to the dark grey, light grey, black and white areas, respectively (Matthews et al., 2020). Furthermore, Science & Grivel (2004) propose that the presence of the MgO layer between MgB_2 grains prevents direct connectivity between the MgB_2 grains. The MgO impurities that occur between the grains limit the migration and diffusion of the various elements during sintering and act as barriers that preventing grain growth. (Guilmeau et al., 2003). The porosities of samples also high with the higher addition of S. based on the SEM images, the sample $MgB_2S_{0.1}$ has the largest grains that produce difficulties to calculate the grain size. The results obtained not agreeing the facts that addition of S into the samples will help to reduce the formation of MgO since S also a non-metal reactant that will react with oxygen and produce Sulphur Dioxide (SO_2). In contrast, the large amount of MgO phase produced causes strong aggregation of MgO particles, weak bonds at grain boundaries, and impediments to the circulation of intergranular supercurrents (Guilmeau et al., 2003).

Figure 4.2.1, figure 4.2.3, figure 4.2.5, figure 4.2.7 and figure 4.2.9 demonstrate the distribution of grain size for each sample. The length of the grains in the sample was measured using the ImageJ software. The grain size distribution was calculated using 100 grains which were chosen randomly. The average grains size for each sample was shown in the figure. Figure 4.2.10 indicates the trend of average grain size for every samples in this study. The average grain size for all samples that contained S with x=0.0, 0.02, 0.05, 0.07 and 0.1 were 0.442μm, 0.438μm, 0.507μm,0.515μm and 0.639μm respectively. According to the results, the average grain size in all samples increases with the number of mol of sulphur added, except for the sample with 0.02mol S addition, which has a lower average grain size when compared to MgB_2 without addition. Sample with 0.1mol addition of S was contribute to very large average grains size compared to other samples. Addition of S could result in decreases the grains size and act as pinning centre that will increases the value of critical current density but no evidence from previous study was found on effect addition S on MgB_2 superconductor.

Guilmeau et al. (2003) propose that the larger the granules, the lower the number of compounds per unit volume. In addition, small particles can bind more closely than large particles. Matthews et al. (2020) proposed that the superbly linked and homogenous bulk sample allow macroscopic currents flow through it. Guilmeau et al. (2003) demonstrate that the intergranular current density was affected by size granules of the samples. Matthews et al. (2020) suggested that the porous, poorly connected microstructure will creates small intragranular supercurrent loops that affect the resistance of the pellets. Higher resistance caused by collision among grains may results the superconducting state of MgB_2 decreased.

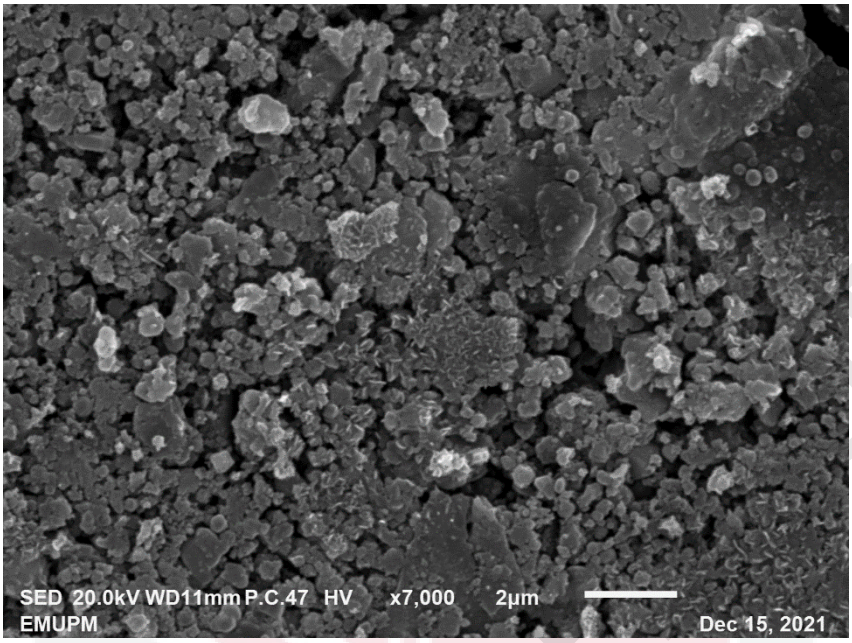

Figure 4.2: SEM images of MgB_2 sintered at 800˚C for 7000x magnification

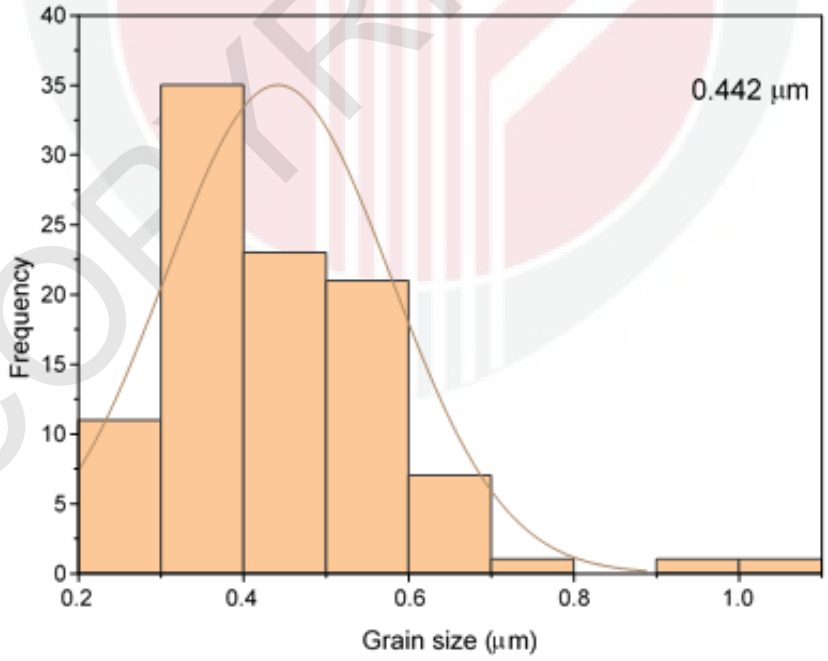

Figure 4.2.1: Grain size distribution of MgB_2 sintered at 800˚C and its average grain size.

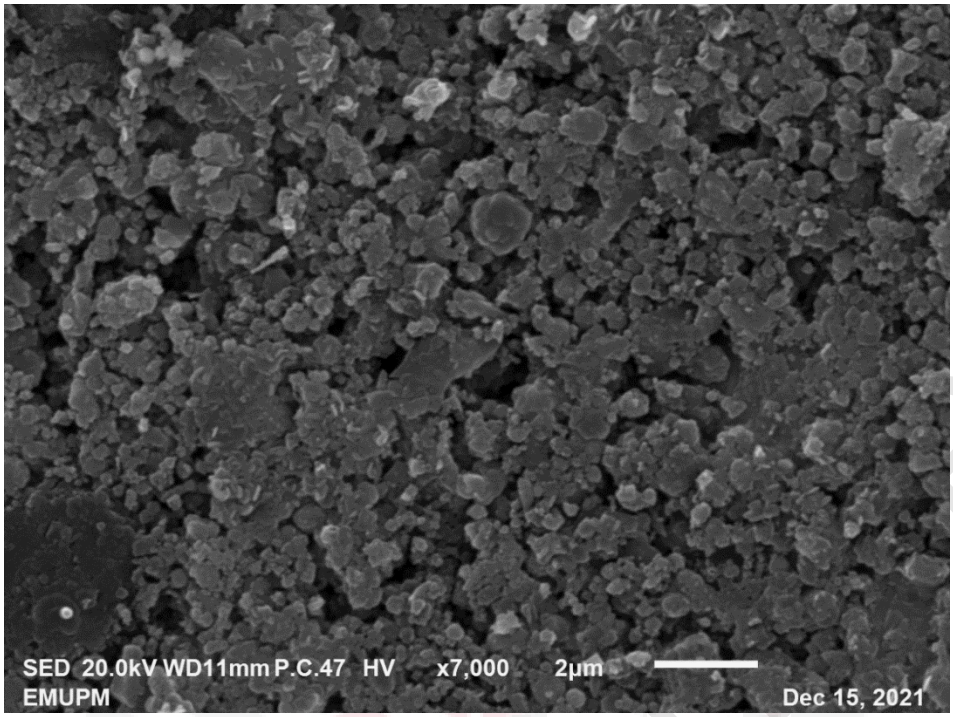

Figure 4.2.2: SEM images of $MgB_2S_{0.02}$ sintered at 800˚C for 7000x magnification

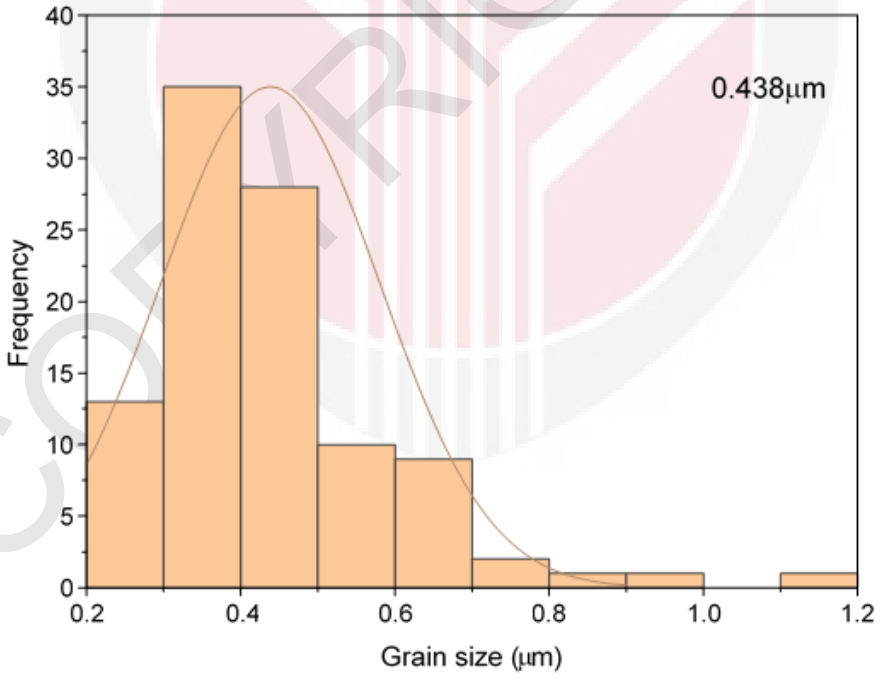

Figure 4.2.3: Grain size distribution of $MgB_2S_{0.02}$ sintered at 800˚C and its average grain size.

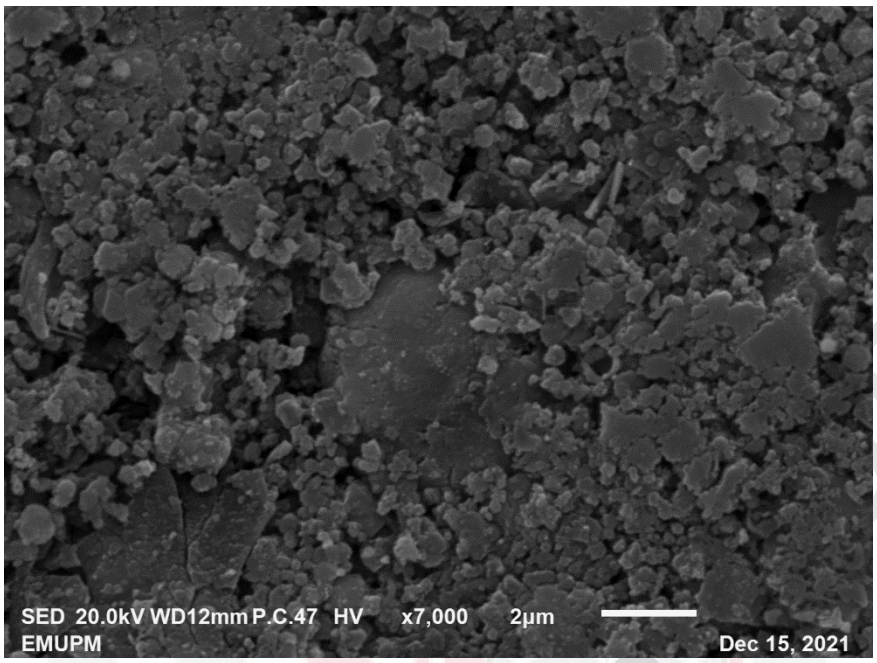

Figure 4.2.4: SEM images of $MgB_2S_{0.05}$ sintered at 800˚C for 7000x magnification

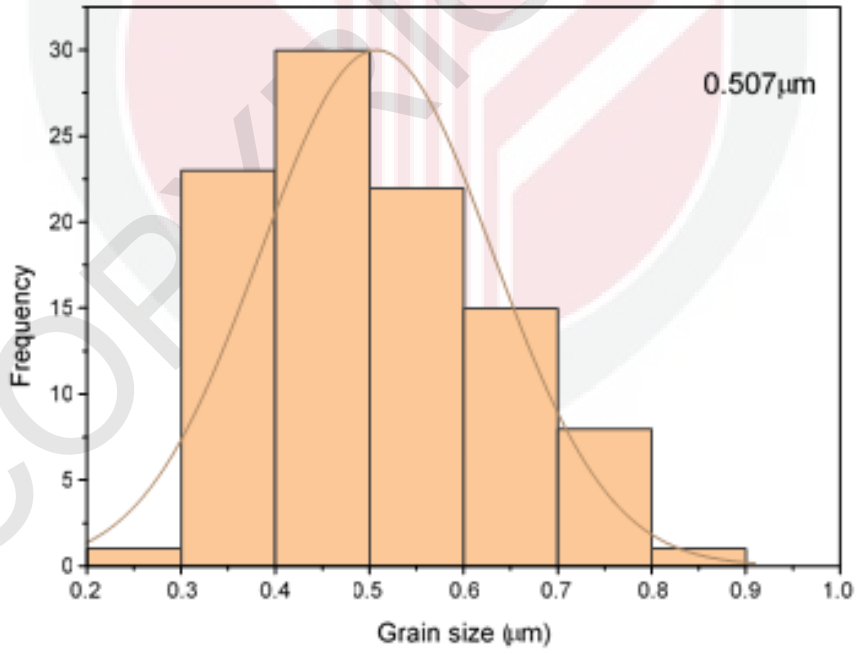

Figure 4.2.5: Grain size distribution of $MgB_2S_{0.05}$ sintered at 800˚C

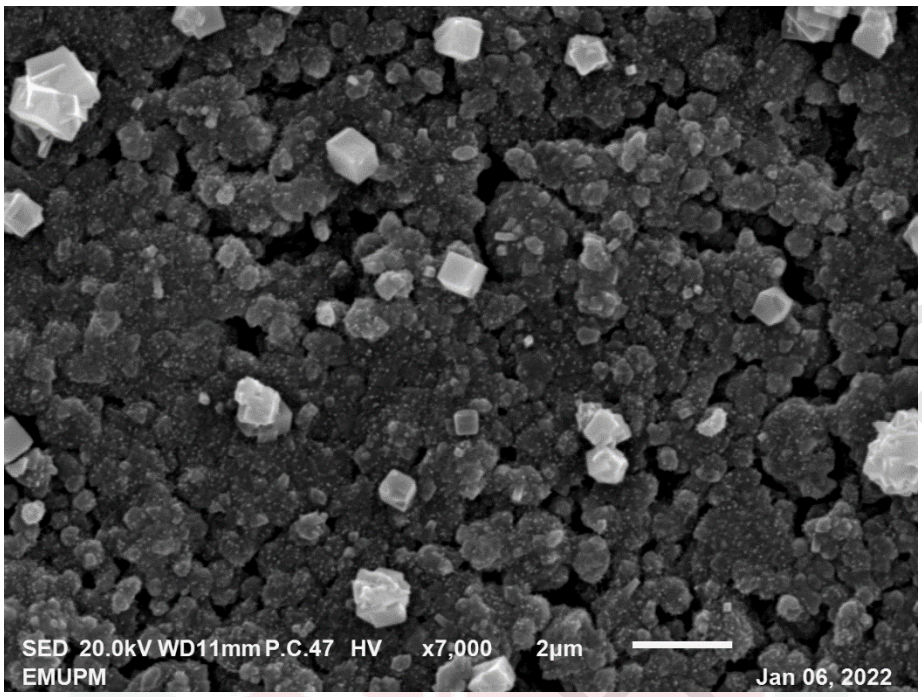

Figure 4.2.6: SEM images of $MgB_2S_{0.07}$ sintered at 800˚C for 7000x magnification

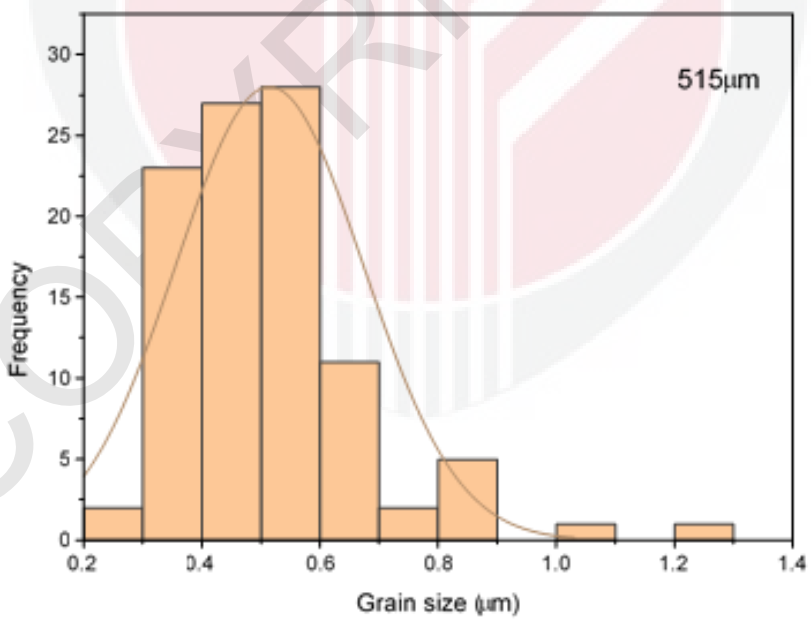

Figure 4.2.7: Grain size distribution of $MgB_2S_{0.07}$ sintered at 800˚C and its average grain size.

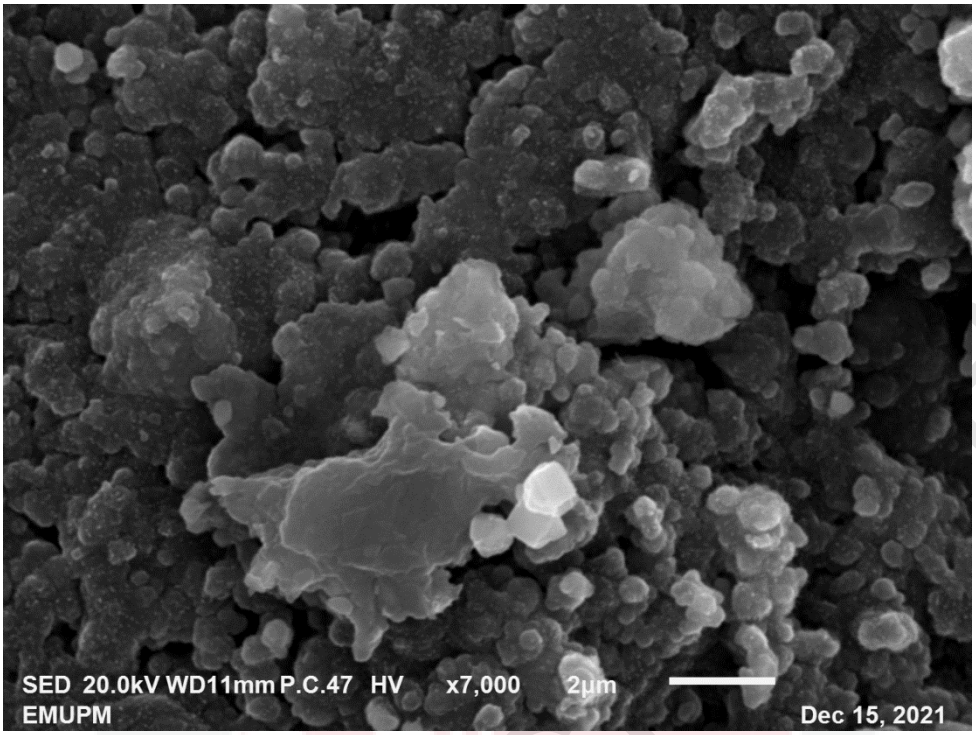

Figure 4.2.8: SEM images of $MgB_2S_{0.10}$ sintered at 800˚C for 7000x magnification

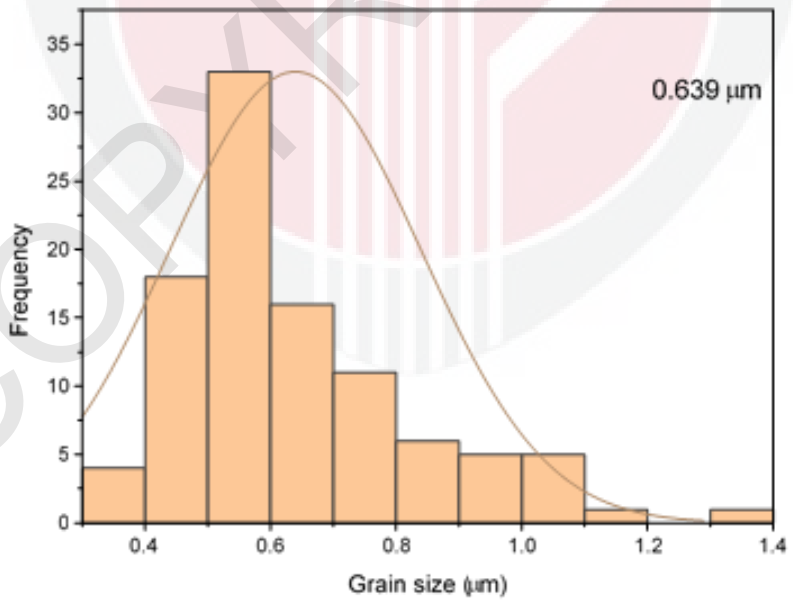

Figure 4.2.9: Grain size distribution of $MgB_2S_{0.1}$ sintered at 800˚C and its average grain size.

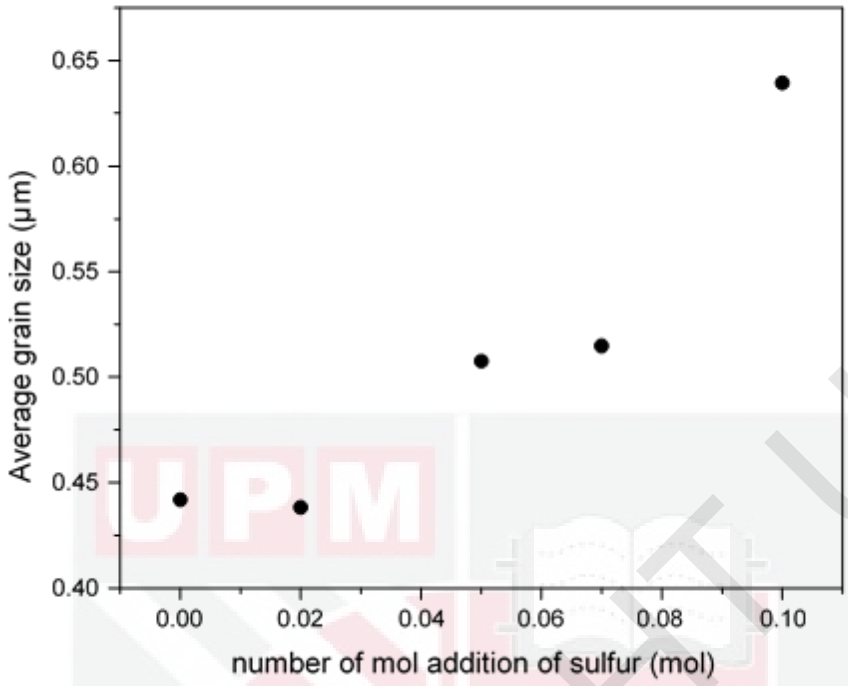

Figure 4.2.10: The average grain size of every samples.

4.3 DENSITY MEASUREMENT

Table 4.2 indicates the density of MgB_2 with and without addition of S. According to table, there are two different ways in determining the density of the samples. By using the densimeter, the mass in air, mass in water and density value of the sample was obtained. By applying the concept of Archimedes Principle, the volume of the sample can be obtained by subtracting the mass of pellet in air with the mass of pellet in water. Then, the density value of the samples was calculated by dividing the mass with the volume of the pellet. The mass of the pellets measured by using electronic digital balance.

However, the density values measured by both ways were quite the same except for the sample with 0.07mol of S addition that have difference by 0.18g/cm^3. The density of MgB_2 without addition of S was determined to be 1.82 g/cm^3. The addition of sulphur by 0.02 mol has the highest density, 1.89 g/cm^3. The decreased value of density proves that the increase of porosity between the grains. This fact agreeing with that reported by (Matthews et al., 2020) that demonstrate that the porous microstructure caused lower value in density due to the volume reduction of MgB_2 formation from the Mg and B phases of the element and the volatility of the Mg powder above the melting point 650 ° C. However, the increase the number of mole S addition, the decrease the density with ranging from 1.89 g/cm^3 to 1.50 g/cm^3. Zhang et al. (2015) investigated that the evaporation of Mg that caused large voids in the bulk leading to a decrease in the sample density. Figure 4.3.1 illustrates the trend of density for all the samples that measured using the densimeter.

Table 4.3: The density values that measured by solid densimeter and calculation based on Archimedes Principle.

Sample	mass in air(g)	mass in water(g)	volume (cm^3)	Density measured by densimeter (g/cm^3)	density calculation (g/cm^3)
MgB_2	0.48	0.22	0.26	1.82	1.85
$MgB_2S_{0.02}$	0.33	0.16	0.17	1.89	1.94
$MgB_2S_{0.05}$	0.36	0.17	0.19	1.86	1.90
$MgB_2S_{0.07}$	0.37	0.13	0.24	1.72	1.54
$MgB_2S_{0.1}$	0.36	0.12	0.24	1.50	1.50

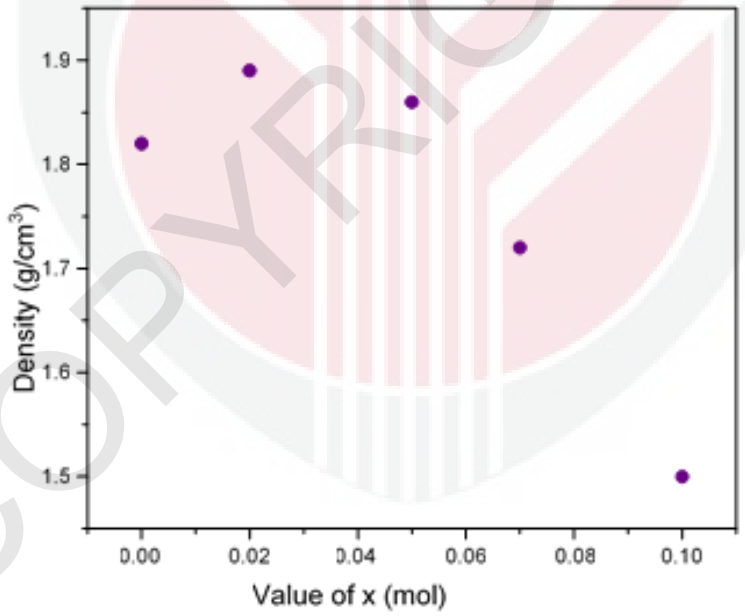

Figure 4.3.1: The density versus type of samples.

CHAPTER 5

CONCLUSION

5.1 CONCLUSION

In this study, there are five samples prepared to study the effects of 0.0, 0.02, 0.05, 0.07 and 0.1 mol of S added to MgB_2. All the pellets were sintered at 800°C in argon furnace for one hour. The samples were characterized by using X-ray Diffraction method (XRD), scanning electron microscope (SEM), density measurement and four-point probe method.

It is concluded that the main phase formed for all samples in this study was MgO and unfortunately MgB_2 acted as secondary phase. the unexpected high presence of MgO probably due many reasons that supported by many researchers. In addition, the S added does contribute to MgB_2 formation in the samples. Plus, the higher mole of S added, the lattice strain and crystallite size were increased. The lattice parameter of a-axis and c-axis were fluctuated with the increasing mass of S added to the sample. However, there only an inadequate differences value among the series of a-axis and c-axis.

Based on the SEM morphology, the hexagonal grains were more distorted and agglomerated as number of moles S added increased. The average size of 100 grains that chosen randomly in each sample increased as number of moles S added increased except for sample with addition 0.02mol S that lower value than sample of MgB_2 without addition.

The density value of the samples measured by solid densimeter were ranging from 1.82 g/cm^3 to 1.50 $g/cm^{3.}$ The density value of the samples was increased until it reaches the optimum value with the addition of sulphur 0.02 mol since it decreases as number of moles S added onward increased. The reduction in density value caused by evaporation of Mg which results in large holes in bulk.

5.2 SUGGESTIONS

The sulphur and Mg powders must undergo XRD analysis to confirm that the powders used are not vaporize and oxidise yet. Plus, the grinding process should be carried in glove box to avoid the reaction of Mg metallic with oxygen hence reduce the formation of MgO. In addition, in order to study further about superconducting in MgB_2, critical current density and grain connectivity should be measured.

REFERENCES

Aksu, E. (2013). Study of MgB2 phase formation by using XRD, SEM, thermal and magnetic measurements. *Journal of Alloys and Compounds*, *552*(March 2013), 376–381. https://doi.org/10.1016/j.jallcom.2012.11.088

Baturina, T., & Vinokur, V. M. (2014). *Ginzburg-Landau Equations*. *3*(May), 4.

Bor, U., Enstitüsü, A., Rafieazad, M., Balcı, Ö., Acar, S., & Somer, M. (2017). JOURNAL OF BORON DERGİSİ Review on magnesium diboride (MgB 2) as excellent superconductor: Effects of the production techniques on the superconducting properties BOR DERGİSİ JOURNAL OF BORON. *Boron*, *2*(2), 87–96. http://dergipark.gov.tr/boron

Buzea, C., & Yamashita, T. (2001). Review of superconducting properties of MgB2. *Cond-Mat*, *1*(1), 13–20.

De Lima, O. F., & Crdoso, C. A. (2003). Anisotropy in MgB2. *Brazilian Journal of Physics*, *33*(4 SPEC. ISS.), 709–712. https://doi.org/10.1590/s0103-97332003000400014

Grivel, J. C., Andersen, N. H., Pallewatta, P. G. A. P., Zhao, Y., & Von Zimmermann, M. (2012). Influence of Bi, Se and Te additions on the formation temperature of MgB 2. *Superconductor Science and Technology*, *25*(1), 5–9. https://doi.org/10.1088/0953-2048/25/1/015010

Guilmeau, E., Andrzejewski, B., & Noudem, J. G. (2003). *The effect of MgO addition on the formation and the superconducting properties of the Bi2223 phase*. *387*(1), 382–390. https://doi.org/10.1016/S0921-4534(02)02360-2

Matthews, G. A. B., Santra, S., Ma, R., Grovenor, C. R. M., Grant, P. S., & Speller, S. C. (2020). Effect of the sintering temperature on the microstructure and superconducting properties of MgB2 bulks manufactured by the field assisted sintering technique. *Superconductor Science and Technology*, *33*(5), 0–11. https://doi.org/10.1088/1361-6668/ab7c53

Pan, A. V., Zhou, S., Liu, H., & Dou, S. (2003). Properties of superconducting MgB2 wires: In situ versus ex situ reaction technique. *Superconductor Science and Technology*, *16*(5), 639–644. https://doi.org/10.1088/0953-2048/16/5/317

Science, S., & Grivel, J. (2004). *The role of MgO content in ex situ MgB 2 wires My IOPscience The role of MgO content in ex situ MgB2 wires*. *17*(October), 43–45. https://doi.org/10.1088/0953-2048/17/10/L03

Serquis, A., Zhu, Y. T., Peterson, E. J., Coulter, J. Y., Peterson, D. E., & Mueller, F. M. (2001). Effect of lattice strain and defects on the superconductivity of MgB2. *Applied Physics Letters*, *79*(26), 4399–4401. https://doi.org/10.1063/1.1428109

Shcherbakov. (2011). Magnesium diboride superconductor : thermal stabilization and doping. *Thesis*, *1*(1), 1–8.

Tanaka, H., Yamamoto, A., Shimoyama, J. I., Ogino, H., & Kishio, K. (2012). Strongly connected exsitu MgB 2 polycrystalline bulks fabricated by solid-state self-sintering. *Superconductor Science and Technology*, *25*(11), 1–10. https://doi.org/10.1088/0953-2048/25/11/115022

Tomsic, M., Rindfleisch, M., Yue, J., Mcfadden, K., Phillips, J., Sumption, M. D., Bhatia, M., Bohnenstiehl, S., & Collings, E. W. (2007). Overview of MgB2 superconductor applications. *International Journal of Applied Ceramic Technology*, *4*(3), 250–259. https://doi.org/10.1111/j.1744-7402.2007.02138.x

Van Delft, D., & Kes, P. (2011). The discovery of superconductivity. *Europhysics News*, *42*(1), 21–25. https://doi.org/10.1051/epn/2011104

Wang, G., Raine, M. J., & Hampshire, D. P. (2017). How resistive must grain boundaries in polycrystalline superconductors be, to limit J c? *Superconductor Science and Technology*, *30*(10), 7–17. https://doi.org/10.1088/1361-6668/aa7f24

Xu, X., Kim, J. H., Hossain, M. S. A., Park, J. S., Zhao, Y., Dou, S. X., Yeoh, W. K., Rindfleisch, M., & Tomsic, M. (2008). Phase transformation and superconducting properties of MgB2 using ball-milled low purity boron. *Journal of Applied Physics*, *103*(2), 103. https://doi.org/10.1063/1.2832752

Xu, Xun, Li, W., Wang, X., & Dou, S.-X. (2011). Superconducting Properties of Graphene Doped Magnesium Diboride. *Applications of High-Tc Superconductivity*, *10*(June), 202–206. https://doi.org/10.5772/17117